

Anisotropic scaling of the two-dimensional Ising model I: The torus

Hendrik Hobrecht^{1*}, Alfred Hucht¹

¹ Fakultät für Physik, Universität Duisburg-Essen
Lotharstr.1, D-47048 Duisburg, Germany

* hendrik@thp.uni-due.de

December 10, 2021

Abstract

We present detailed calculations for the partition function and the free energy of the finite two-dimensional Ising model with periodic and antiperiodic boundary conditions, variable aspect ratio, and anisotropic couplings on the square lattice, as well as for the corresponding free energy scaling functions. Therefore we discuss the dimer mapping, the interplay between its topology and the different types of boundary conditions. As a central result we show how both the finite system as well as the scaling form decay into contributions for the bulk, a characteristic finite-size part, and – if present – the surface tension and its emergence due to at least one antiperiodic boundary in the system. For the scaling limit we expand the proper finite-size scaling theory to the anisotropic case and show how this anisotropy can be absorbed into suitable scaling variables.

Contents

1	Introduction	2
2	The dimer representation	3
2.1	Dimers	5
2.2	Translational invariance	8
3	Scaling theory	12
3.1	General scaling behaviour	14
3.2	Anisotropic scaling	15
4	The torus	16
4.1	Bulk and finite-size contribution	17
4.2	Scaling form	19
4.3	(Anti-)Periodicity and surface tension	25
5	Conclusion	27
	References	28

1 Introduction

The two-dimensional Ising model is by far the most examined and best understood non-trivial system in statistical physics. Albeit there are still open questions, there is a whole plethora of properties known exactly, starting with the exact partition function on the torus in the thermodynamic limit with no magnetic field calculated by Onsager [1], over the universal finite-size scaling at its continuous phase transition from a ferromagnetic low-temperature to a paramagnetic high-temperature phase [2, 3], to the exact solutions at criticality due to conformal field theory for arbitrary geometries and boundary conditions (BCs) [4–7]. There are as much ways to calculate all these properties as there are people working on the topic, but a few are truly worth mentioning here. Beneath Onsager’s expansion of the transfer matrix calculation to two dimensions, there are at least two major ideas, which are repeatedly used over last decades; one is the mapping onto spinors, as done lately by Baxter for the case of a rectangular geometry with open boundaries [8] and originally introduced by Kaufman [9]. The other one is the dimer mapping, introduced by Kasteleyn, refined by Fisher [10], and rigorously and exhaustively examined by McCoy and Wu [11]. The latter one will be our starting point and we will be putting a lot of effort into its analysis relating the topology of the underlying graph and the boundary conditions of the spin system. Boundaries that destroy the translational invariance in one direction and additional surface fields will be the topic of the subsequent part of this paper [12].

The original inspiration for this work lies within the aforementioned universal finite-size scaling; in the vicinity of criticality the behaviour of many systems can be sorted into an according universality class, categorised only by some rough properties like its spacial and spin dimensions, and split up into subcategories treating the BCs confining the system. Accompanying the universality, the diverging correlation length $\xi^{(\infty)}$ at criticality in finite systems gives rise to the thermodynamic analogue of the quantum-electrodynamics (QED) Casimir effect [13, 14], predicted by Fisher and de Gennes [15]. The critical fluctuations present in such a geometrically confined system lead to an effective force between the systems surfaces: The critical Casimir force. In contrast to the always attractive QED Casimir effect, these thermal forces may be attractive or repulsive depending on the BCs of the surfaces, and can even change their behaviour with the temperature. This fact together with its steering temperature dependence makes them especially interesting as experimental model systems, e.g., they may be used to control the interaction strength in colloidal suspensions in order to investigate the aggregation processes. The effect itself was first measured by Garcia and Chan as a critical thinning of a ^4He film near the λ -transition [16]. The universality of this measurement was first proven by Monte Carlo simulations of the XY -model in three dimensional thin films with Dirichlet boundary conditions [17]. Other systems experiments were made on are thin films of ^3He - ^4He mixtures near the tricritical point [18], again in the XY -universality class, and binary liquids, whose demixing transition is in the Ising-universality class [19]. The latter experimental system was expanded to the direct measurement of interactions between spherical particles and a potentially chemically striped surface as well as the observation of aggregation processes in the above-mentioned colloidal suspensions [20].

As the analytical point of view of those systems is either restricted to mean-field calculations [21], the large- n limit [22, 23], or calculations at criticality, where the systems conformal invariance opens up some fascinating possibilities [24–27], there are many works on Monte Carlo simulations of such systems [17, 28]. Starting with the original slab geometry, where some sort of thermodynamic integration is necessary to obtain the free energy, they were lately expanded to spherical objects [29–31], which establishes the opportunity to implement the same protocols for a direct measurement of the free energies due to the probability distributions of the positions of the objects.

For this work, in Section 2 we first recapitulate the mapping between the two-dimensional Ising model and closest-packed dimers on a carefully chosen lattice proposed by Kasteleyn and expand the argumentation to arbitrary nearest-neighbour couplings between each pair of sites. Therefore we will refine the argumentation by McCoy & Wu and, in contrast to the calculations for the rectangular system with open boundary conditions, we will implement translational invariance in one direction to simplify the problem further, which leaves us with the toroidal and the cylindrical topology, where the latter one will be the topic of the subsequent part of this paper. Allowing anisotropic couplings we will show how the introduction of the dual coupling leads to a much more natural calculation than in [32]. Later on, the general calculation of the emerging determinant gives us the opportunity to implement several different boundary conditions, but also makes a recapitulation of the scaling theory necessary, especially for the anisotropic case, which will be done in Section 3. Here we will also recapitulate the relation between the different points of view concerning the preferred direction within the system, e. g., the direction in which the critical Casimir force is measured, as well as the relations between the scaling functions for the free energy and the critical Casimir force. Afterwards we will start with the calculation of the partition function for the anisotropic toroidal case in Section 4, which will be a crucial point for the calculation for the symmetric symmetry-breaking $(++)$ and the asymmetric symmetry-breaking $(+-)$ boundaries in the subsequent paper, as it enlightens the interdependency of the dimer mapping and the distinction of periodic and anti-periodic boundary conditions and lets us identify the bulk contribution, which is present in every case we are going to examine later on. We apply the anisotropic scaling theory to the Onsager dispersion to obtain the scaling forms of the relevant terms and introduce its hyperbolic parametrisation, which allows us to regularise the infinite sums by rewriting them as contour integrals over singly periodic functions in the complex plane, giving a modified Abel-Plana formula, and reproduce the free energy scaling function for the toroidal case [32–34]. With at least one antiperiodic boundary the system forms a domain wall, which introduces the surface tension as contribution to the residual free energy, giving us a first glimpse on its general form. The cylindric geometry and boundary field effects will be discussed elsewhere.

2 The dimer representation

We will start with a brief summary of the dimer representation of the two-dimensional Ising model as it was introduced by Kasteleyn and refined by Fisher, as well as an explanation of how the according matrices are constructed. Then we will assume translational invariance in one direction and reduce the calculation of the determinant successively by two Schur reductions. This makes it convenient to introduce the dual couplings, which lead to a more readable and

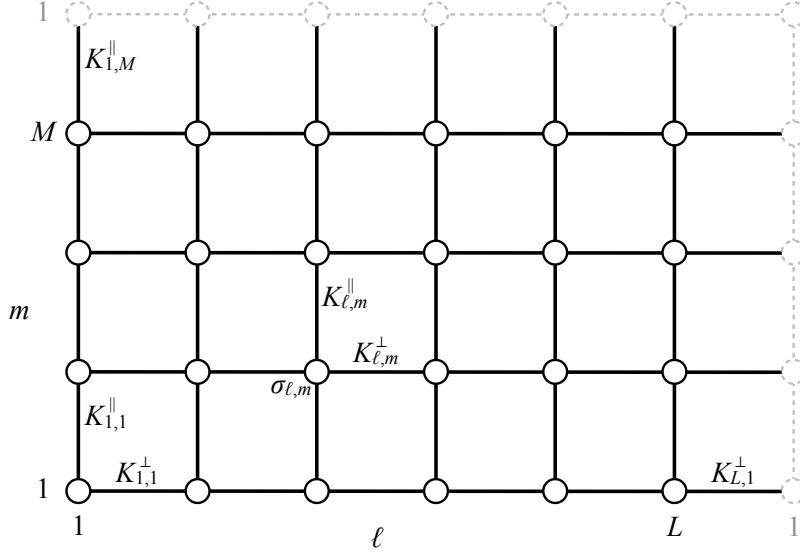


Figure 1: The square lattice with toroidal geometry for $M = 4$ and $L = 6$.

natural form. Eventually we obtain the determinant of a (quasi-)cyclic tridiagonal matrix, which can be calculated in terms of a simple 2×2 transfer matrix. This step will be our starting point for all further calculations, as the various BCs can be simply introduced in the reduced matrix and thus form such 2×2 matrices for the boundary terms. Finally we assume translational invariance in both direction, reproducing the result of McCoy & Wu.

The classical two-dimensional Ising model on an $L \times M$ square lattice with periodic boundary conditions (p) in both directions as depicted in Fig. 1, i. e., on the torus, has the reduced Hamiltonian (in units of $k_B T$ with Boltzmann constant k_B)

$$\mathcal{H}^{(p,p)} = - \sum_{\ell=1}^L \sum_{m=1}^M K_{\ell,m}^{\perp} \sigma_{\ell,m} \sigma_{\ell+1,m} - \sum_{\ell=1}^L \sum_{m=1}^M K_{\ell,m}^{\parallel} \sigma_{\ell,m} \sigma_{\ell,m+1}, \quad (1)$$

where $K_{\ell,m}^{\perp}$ and $K_{\ell,m}^{\parallel}$ are the reduced couplings between the nearest neighbours in perpendicular and parallel direction, respectively, and $\sigma_{\ell,m} \in \{-1, +1\}$ are spin variables with periodic indices, i. e., $\sigma_{\ell+L,m} \equiv \sigma_{\ell,m}$ and $\sigma_{\ell,m+M} \equiv \sigma_{\ell,m}$. The partition function $Z^{(p,p)} = \text{tr} e^{-\mathcal{H}^{(p,p)}}$ can be rewritten into a high-temperature expansion

$$\frac{Z^{(p,p)}}{Z_0^{(p,p)}} = \frac{1}{2^{LM}} \sum_{\{\sigma\}} \prod_{\ell=1}^L \prod_{m=1}^M \left(1 + z_{\ell,m}^{\perp} \sigma_{\ell,m} \sigma_{\ell+1,m} \right) \prod_{\ell=1}^L \prod_{m=1}^M \left(1 + z_{\ell,m}^{\parallel} \sigma_{\ell,m} \sigma_{\ell,m+1} \right), \quad (2)$$

with $z_{\ell,m}^{\delta} = \tanh K_{\ell,m}^{\delta}$ ($\delta = \perp, \parallel$), as well as with the non-singular part

$$Z_0^{(p,p)} = \prod_{\ell=1}^L \prod_{m=1}^M 2 \cosh K_{\ell,m}^{\perp} \cosh K_{\ell,m}^{\parallel}. \quad (3)$$

Here we used the identity

$$e^{K \sigma_i \sigma_j} = \cosh K + \sigma_i \sigma_j \sinh K, \quad (4)$$

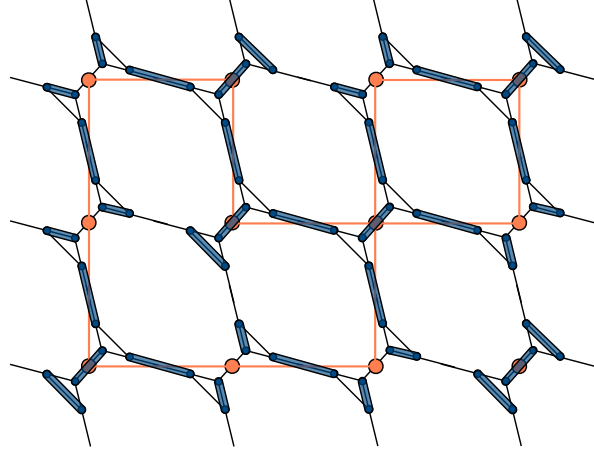


Figure 2: Example for the dimer representation of the graphical interpretation of the partition function on a $(L = 4) \times (M = 3)$ lattice. The original lattice sites are depicted as large circles, while the orange lines are an exemplary polygon configuration. All eight possible dimer configurations can be seen. The term in the sum in (2) is $z_{1,1}^\perp z_{2,1}^\perp z_{2,2}^\perp z_{3,2}^\perp z_{1,3}^\perp z_{3,3}^\perp z_{1,1}^\parallel z_{1,2}^\parallel z_{2,2}^\parallel z_{3,1}^\parallel z_{3,2}^\parallel z_{4,2}^\parallel$.

as $\sigma_i \sigma_j = \pm 1$ depending on whether the spins are aligned or unaligned.

Expanding the sum and both products leaves only even powers of the $\sigma_{\ell,m}$, which are always equal to one, and a factor of 2^{LM} , which we already included in $Z_0^{(p,p)}$. This can be interpreted as follows: Each term in the sum gives a possible configuration of closed and commonly intersecting polygons on the original lattice, where every $z_{\ell,m}^\perp$ gives the position of a perpendicular and every $z_{\ell,m}^\parallel$ a parallel link that has to be drawn, see Fig. 2 for an example.

2.1 Dimers

If we replace each site of the lattice with a properly chosen cluster, this problem is equivalent to finding the generating function of the closest-packed dimer configuration on the expanded lattice. In this context a dimer is a two-atomic construct, which always occupies two sites and the connecting bond of the lattice. Fisher introduced a six-site cluster as depicted in Fig. 3(a) for this replacement, which can be further reduced to a four-site cluster, see Fig. 3(b). The dimers can be arranged in such a way that they reflect the polygon structure in a biunique way occupying either a original lattice edge or lying within the cluster, thus leaving the edge unoccupied, see again Fig. 2.

The problem of finding the generating function of the closest-packed dimer configurations on an arbitrary planar graph was solved by Kasteleyn in terms of Pfaffians, as it gives the number of *perfect matchings* of a given directed planar graph with an even number of sites. This is especially powerful because of the connection between the Pfaffian and the determinant, namely

$$(\text{Pf } \mathcal{A})^2 = \det \mathcal{A}. \quad (5)$$

To apply this method, we have to construct a suitable skew-symmetric matrix, which corresponds to the directed graph of the lattice; the construction of this matrix will be the topic of this section. The directed graph we need has to fulfil some restrictions, the most important

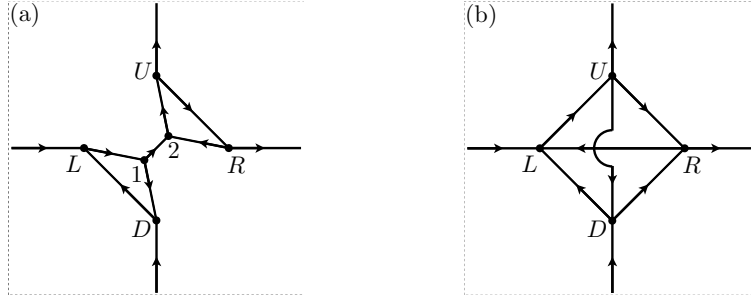


Figure 3: The six-site (a) and the four-site (b) cluster that may be used to expand the lattice for the dimer mapping.

and fundamental being that each elementary polygon is *clockwise odd*, that is, the number of edges pointing in clockwise direction has to be odd. This is naturally satisfied for the cluster expanded lattice and guarantees that every term in the Pfaffian will have the same sign on any given planar graph. Consequently, for the toroidal topology of the original lattice, one Pfaffian is not sufficient, since the argument aforementioned originates in the need that every *transitions cycle*, which describes the transition from one dimer configuration to another, needs to be odd, see [11, Chapter 4.3-4.5] for details. On a torus this cannot be accomplished by a single but by a superposition of four Pfaffians, corresponding to the four possible combinations of periodic and anti-periodic boundary conditions in the two directions, that cancels out the redundant terms and besides gives the correct signs for the transition cycles that wind around the torus in either or both directions. These four combinations of periodic and anti-periodic BCs are implemented by reversing the direction of the directed graphs in the lines responsible for the periodicity. This last point will be discussed in detail in Section 4, where the interplay of the dimer mapping and periodic and anti-periodic boundaries will be discussed in more detail, and later on in the upcoming second part of this paper, where we will distinguish the $(++)$ and the $(+-)$ boundary conditions as being periodic and anti-periodic in the perpendicular direction.

To construct the matrix we will first take a look at the adjacency matrix of the graph, which decomposes into the clusters replacing the original sites and the two direction of the lattice. Using the common labels for the cluster as shown in Fig. 3(a), the graph can be represented as

$$C_6^0 = \begin{matrix} & R & L & 1 & 2 & U & D \\ \begin{matrix} R \\ L \\ 1 \\ 2 \\ U \\ D \end{matrix} & \begin{pmatrix} 0 & 0 & 0 & 1 & 0 & 0 \\ 0 & 0 & 1 & 0 & 0 & 0 \\ 0 & 0 & 0 & 1 & 0 & 1 \\ 0 & 0 & 0 & 0 & 1 & 0 \\ 1 & 0 & 0 & 0 & 0 & 0 \\ 0 & 1 & 0 & 0 & 0 & 0 \end{pmatrix} \end{matrix}. \quad (6)$$

To simplify the problem further, the graph can be reduced into a non-planar one with only four sites, eliminating the two interior sites labeled 1 and 2, e.g. as the Schur complement (25) of the antisymmetric form of (6) with respect to the central 2×2 block. The according

cluster is depicted in Fig. 3(b) and its adjacency matrix is

$$\mathbf{C}_4^0 = \begin{matrix} & R & L & U & D \\ \begin{matrix} R \\ L \\ U \\ D \end{matrix} & \begin{pmatrix} 0 & 1 & 0 & 0 \\ 0 & 0 & 1 & 0 \\ 1 & 0 & 0 & 1 \\ 1 & 1 & 0 & 0 \end{pmatrix} \end{matrix}. \quad (7a)$$

Nevertheless, this reduction introduces two additional terms for each lattice site of the original system that is not part of any polygon, as there are now three combinations on the Kasteleyn cluster for those cases. But if each bond within the clusters has a weight equal to 1 those additional terms cancel each other and we ensure that no cluster has an influence on (2). On this resolution, the coupling in parallel and perpendicular direction are covered by the two matrices

$$\mathbf{C}_4^{\parallel} = \begin{matrix} & R & L & U & D \\ \begin{matrix} R \\ L \\ U \\ D \end{matrix} & \begin{pmatrix} 0 & 1 & 0 & 0 \\ 0 & 0 & 0 & 0 \\ 0 & 0 & 0 & 0 \\ 0 & 0 & 0 & 0 \end{pmatrix} \end{matrix} \quad (7b)$$

and

$$\mathbf{C}_4^{\perp} = \begin{matrix} & R & L & U & D \\ \begin{matrix} R \\ L \\ U \\ D \end{matrix} & \begin{pmatrix} 0 & 0 & 0 & 0 \\ 0 & 0 & 0 & 0 \\ 0 & 0 & 0 & 1 \\ 0 & 0 & 0 & 0 \end{pmatrix} \end{matrix}, \quad (7c)$$

respectively. The nearest-neighbour structure in a row and a column are both covered by the $n \times n$ matrix

$$\mathbf{H}_{\mathbf{b},n} = \begin{pmatrix} 0 & 1 & 0 & \cdots & 0 \\ 0 & 0 & 1 & & 0 \\ \vdots & & & \ddots & \vdots \\ 0 & 0 & 0 & & 1 \\ \mathbf{b} & 0 & 0 & \cdots & 0 \end{pmatrix}, \quad (8)$$

with $\mathbf{b} \in \{+1, 0, -1\}$ accounting for different BCs, i.e., $\mathbf{b} = 0$ for open, $\mathbf{b} = -1$ for periodic, and $\mathbf{b} = +1$ for anti-periodic boundaries of the Ising system, concerning the necessity of transition cycles on the graph to be odd. Note, that $\mathbf{b} = +1$ accounts for periodic boundaries on the directed graph, i.e., in the dimer system, in the sense that all edges are likewise aligned. Nevertheless, the topology of the underlying directed graph is not representative for the emulated Ising model, which is emphasised by the fact that the Ising partition function is a combination of four Pfaffians. The identification with periodicity and antiperiodicity for the values of \mathbf{b} stems solely from the identification within the open cylinder, see [12, 32]. If we

give each bond a different weight, see Fig. 1, we can represent the parallel and perpendicular couplings by

$$\mathbf{Z}_\alpha^\perp = \mathbf{Z}^\perp (\mathbf{H}_{\alpha,L} \otimes \mathbf{1}_M), \quad (9a)$$

$$\mathbf{Z}_\beta^\parallel = \mathbf{Z}^\parallel (\mathbf{1}_L \otimes \mathbf{H}_{\beta,M}), \quad (9b)$$

with $\mathbf{Z}^\delta = \text{diag}(z_{1,1}^\delta, z_{1,2}^\delta, \dots, z_{L,M}^\delta)$ and the $n \times n$ identity matrix $\mathbf{1}_n$. The final $4LM \times 4LM$ adjacency matrix of the graph then reads

$$\mathbf{A}_{\alpha\beta} = \mathbf{C}_4^0 \otimes \mathbf{1}_{LM} + \mathbf{C}_4^\perp \otimes \mathbf{Z}_\alpha^\perp + \mathbf{C}_4^\parallel \otimes \mathbf{Z}_\beta^\parallel \quad (10)$$

and, since two vertices are connected at most by a single edge, we can expand it to a skew-symmetric block form¹

$$\mathcal{A}_{\alpha\beta} = \mathbf{A}_{\alpha\beta} - \mathbf{A}_{\alpha\beta}^\top = \begin{bmatrix} \mathbf{0} & \mathbf{1} + \mathbf{Z}_\beta^\parallel & -\mathbf{1} & -\mathbf{1} \\ -(\mathbf{1} + \mathbf{Z}_\beta^\parallel)^\top & \mathbf{0} & \mathbf{1} & -\mathbf{1} \\ \mathbf{1} & -\mathbf{1} & \mathbf{0} & \mathbf{1} + \mathbf{Z}_\alpha^\perp \\ \mathbf{1} & \mathbf{1} & -(\mathbf{1} + \mathbf{Z}_\alpha^\perp)^\top & \mathbf{0} \end{bmatrix} \quad (11)$$

to calculate the partition function of the torus as

$$\frac{Z^{(\mathbf{p},\mathbf{p})}}{Z_0^{(\mathbf{p},\mathbf{p})}} = \frac{1}{2} (-\text{Pf } \mathcal{A}_{++} + \text{Pf } \mathcal{A}_{+-} + \text{Pf } \mathcal{A}_{-+} + \text{Pf } \mathcal{A}_{--}). \quad (12)$$

2.2 Translational invariance

Since we are interested only in the boundary conditions along the parallel direction, we now assume translational invariance in this direction (the Ising model on the rectangle with open boundaries in both directions is discussed in [8, 35, 36]). Thus all couplings in one column are the same, i. e., $z_{\ell,m}^\delta \equiv z_\ell^\delta \forall m$ and the matrices \mathbf{Z}^δ simplify to

$$\mathbf{Z}^\delta = z_L^\delta \otimes \mathbf{1}_M, \quad \delta = \parallel, \perp, \quad (13)$$

with $z_L^\delta = \text{diag}(z_1^\delta, \dots, z_L^\delta)$. Additionally we note that \mathbf{H}_b is a normal matrix for $b = \pm 1$ and therefore commutes with its transposed,

$$\mathbf{H}_\pm \mathbf{H}_\pm^\top - \mathbf{H}_\pm^\top \mathbf{H}_\pm = \mathbf{0}, \quad (14)$$

and thus the unitary matrix \mathbf{U}_\pm that diagonalises \mathbf{H}_\pm also does so for \mathbf{H}_\pm^\top . For convenience we decompose the matrix $\mathcal{A}_{\alpha\beta}$ into its three contributions (10) as

$$\mathcal{A}_{\alpha\beta} = \mathcal{A}^0 + \mathcal{A}_\alpha^\perp + \mathcal{A}_\beta^\parallel, \quad (15)$$

where

$$\mathcal{A}^0 = \mathbf{C}_4^0 \otimes \mathbf{1}_L \otimes \mathbf{1}_M - (\text{transposed}), \quad (16a)$$

$$\mathcal{A}_\alpha^\perp = \mathbf{C}_4^\perp \otimes (z_L^\perp \mathbf{H}_{\alpha,L}) \otimes \mathbf{1}_M - (\text{transposed}), \quad (16b)$$

$$\mathcal{A}_\beta^\parallel = \mathbf{C}_4^\parallel \otimes z_L^\parallel \otimes \mathbf{H}_{\beta,M} - (\text{transposed}). \quad (16c)$$

¹In the following we drop the size subscript from matrices if it can be derived from the context.

In the expanded space, $U_{\beta=\pm}$ becomes

$$\mathcal{U}_\beta = \mathbf{1}_4 \otimes \mathbf{1}_L \otimes U_{\beta,M} \quad (17)$$

and has no influence on the first two contributions as they commute,

$$\mathcal{A}^0 \mathcal{U}_\beta - \mathcal{U}_\beta \mathcal{A}^0 = \mathbf{0}, \quad (18a)$$

$$\mathcal{A}_\alpha^\perp \mathcal{U}_\beta - \mathcal{U}_\beta \mathcal{A}_\alpha^\perp = \mathbf{0}. \quad (18b)$$

For the parallel contribution, we obtain the diagonal matrices

$$U_\beta^{-1} \mathbf{H}_\beta U_\beta = \text{diag}\left(e^{+i\varphi_0^{(\beta)}}, \dots, e^{+i\varphi_{M-1}^{(\beta)}}\right), \quad (19a)$$

$$U_\beta^{-1} \mathbf{H}_\beta^\top U_\beta = \text{diag}\left(e^{-i\varphi_0^{(\beta)}}, \dots, e^{-i\varphi_{M-1}^{(\beta)}}\right), \quad (19b)$$

with

$$\varphi_m^{(\beta)} = \begin{cases} 2m\pi/M & \text{if } \beta = +1 \\ (2m+1)\pi/M & \text{if } \beta = -1 \end{cases} \quad (20)$$

for $m \in \{0, 1, 2, \dots, M-1\}$, and thus we will call $\beta = +1$ *even* and $\beta = -1$ *odd*. Note that the eigenvalues lie equidistantly on the unit circle and thus we have a free shifting parameter for the spectrum. We have chosen it in such a way, that the eigenvalue $\varphi_0^{(+)} = 0$ appears in the even spectrum; a shift by $-\pi$ on the other hand would have given rise to a dependency on whether M is even or odd. For completeness we present the characteristic polynomials

$$\mathcal{P}_\beta^\pm(M; \varphi) = \prod_{m=0}^{M-1} \left(e^{\pm i\varphi} - e^{i\varphi_m^{(\beta)}} \right) = e^{\pm iM\varphi} - \beta \quad (21)$$

here, as we will need them later, too. Note that we have chosen to use the normalised version of \mathcal{P}_β^\pm to omit the aforementioned dependency on whether M is even or odd.

Since $\det(\mathbf{A} \otimes \mathbf{B}) = \det(\mathbf{B} \otimes \mathbf{A})$, we can rearrange the matrices such that the product is block diagonal, simplifying its determinant to the form

$$\det \mathcal{A}_{\alpha\beta} = \prod_{m=0}^{M-1} \det \mathcal{B}_\alpha(\varphi_m^{(\beta)}) \quad (22)$$

with the $4L \times 4L$ block matrices

$$\mathcal{B}_\alpha(\varphi_m^{(\beta)}) = \begin{bmatrix} \mathbf{0} & \mathbf{J}_\beta^+ & -\mathbf{1} & -\mathbf{1} \\ -\mathbf{J}_\beta^- & \mathbf{0} & \mathbf{1} & -\mathbf{1} \\ \mathbf{1} & -\mathbf{1} & \mathbf{0} & \mathbf{J}_\alpha \\ \mathbf{1} & \mathbf{1} & -\mathbf{J}_\alpha^\top & \mathbf{0} \end{bmatrix}, \quad (23)$$

where we defined $\mathbf{J}_\alpha = \mathbf{1} + \mathbf{z}^\perp \mathbf{H}_\alpha$ for the perpendicular direction and the diagonal matrices $\mathbf{J}_\beta^\pm = \mathbf{1} + \mathbf{z}^\parallel e^{\pm i\varphi_m^{(\beta)}}$ for the parallel one.

At this point we introduce the dual couplings t_ℓ , which can be defined within the low-temperature expansion of the partition function analogous to (2), but on the dual lattice. They are connected to the couplings z_ℓ^\parallel via the duality transformation

$$t_\ell \equiv (z_\ell^\parallel)^* \equiv \frac{1 - z_\ell^\parallel}{1 + z_\ell^\parallel}, \quad (24)$$

making the distinction between the parallel and the perpendicular direction obsolete. Thus we will omit the superscripts in the following and write $z_\ell \equiv z_\ell^\perp$ and rewrite the parallel couplings z_ℓ^\parallel through their duals t_ℓ^* . In the following we will, if necessary, mark a dual coupling by an asterisk as shown in (24). Consequently we may also rewrite the two matrices $z^\perp \mapsto z$ and $z^\parallel \mapsto t^*$.

As shown in [32] the determinant of the matrix $\mathcal{B}_\alpha(\varphi_m^{(\beta)})$ can be reduced further by two successive Schur reductions according to

$$\det \begin{bmatrix} \mathbf{a}_{11} & \mathbf{a}_{12} \\ \mathbf{a}_{21} & \mathbf{a}_{22} \end{bmatrix} = \det \mathbf{a}_{11} \det (\mathbf{a}_{22} - \mathbf{a}_{21} \mathbf{a}_{11}^{-1} \mathbf{a}_{12}), \quad (25)$$

where we will make the reduction with respect to upper left 2×2 block matrix, as for the first step this part solely represents the couplings in the translationally invariant, parallel direction. The first reduction gives

$$\det \mathcal{B}_\alpha(\varphi_m^{(\beta)}) = \det \begin{bmatrix} \mathbf{0} & \mathbf{J}_\beta^+ \\ -\mathbf{J}_\beta^- & \mathbf{0} \end{bmatrix} \det \begin{bmatrix} -\mathbf{\Delta}_\beta & \mathbf{J}_\alpha - \mathbf{\Sigma}_\beta \\ \mathbf{\Sigma}_\beta - \mathbf{J}_\alpha^\top & \mathbf{\Delta}_\beta \end{bmatrix}, \quad (26)$$

with the matrices $\mathbf{\Sigma}_\beta = (\mathbf{J}_\beta^+)^{-1} + (\mathbf{J}_\beta^-)^{-1}$ and $\mathbf{\Delta}_\beta = (\mathbf{J}_\beta^+)^{-1} - (\mathbf{J}_\beta^-)^{-1}$. As both \mathbf{J}_β^\pm are diagonal, the first determinant simply becomes

$$\det \begin{bmatrix} \mathbf{0} & \mathbf{J}_\beta^+ \\ -\mathbf{J}_\beta^- & \mathbf{0} \end{bmatrix} = \prod_{\ell=1}^L \left(1 + t_\ell^* e^{i\varphi_m^{(\beta)}} \right) \left(1 + t_\ell^* e^{-i\varphi_m^{(\beta)}} \right). \quad (27)$$

For the second determinant in (26) we apply a second Schur reduction with respect to the upper left block matrix, which yields

$$\det \begin{bmatrix} -\mathbf{\Delta}_\beta & \mathbf{J}_\alpha - \mathbf{\Sigma}_\beta \\ \mathbf{\Sigma}_\beta - \mathbf{J}_\alpha^\top & \mathbf{\Delta}_\beta \end{bmatrix} = \det (-\mathbf{\Delta}_\beta) \det \left[\mathbf{\Delta}_\beta + (\mathbf{\Sigma}_\beta - \mathbf{J}_\alpha^\top) \mathbf{\Delta}_\beta^{-1} (\mathbf{J}_\alpha - \mathbf{\Sigma}_\beta) \right]. \quad (28)$$

Again, the first determinant is rather simple,

$$\det (-\mathbf{\Delta}_\beta) = \prod_{\ell=1}^L \left(\frac{1}{1 + t_\ell^* e^{-i\varphi_m^{(\beta)}}} - \frac{1}{1 + t_\ell^* e^{i\varphi_m^{(\beta)}}} \right), \quad (29)$$

and can be combined with (27) to

$$\det (-\mathbf{\Delta}_\beta) \det \begin{bmatrix} \mathbf{0} & \mathbf{J}_\beta^+ \\ -\mathbf{J}_\beta^- & \mathbf{0} \end{bmatrix} = \prod_{\ell=1}^L 2it_\ell^* \sin \varphi_m^{(\beta)}. \quad (30)$$

We finally find

$$\det \mathcal{B}_\alpha(\varphi_m^{(\beta)}) = \det \tilde{\mathcal{C}}_\alpha(\varphi_m^{(\beta)}) \prod_{\ell=1}^L 2t_\ell^* \quad (31)$$

with

$$\tilde{\mathcal{C}}_{\alpha}(\varphi_m^{(\beta)}) = i \sin \varphi_m^{(\beta)} \left[\mathbf{\Delta}_{\beta} + (\mathbf{\Sigma}_{\beta} - \mathbf{J}_{\alpha}^{\dagger}) \mathbf{\Delta}_{\beta}^{-1} (\mathbf{J}_{\alpha} - \mathbf{\Sigma}_{\beta}) \right]. \quad (32)$$

The $L \times L$ matrix $\tilde{\mathcal{C}}_{\alpha}(\varphi_m^{(\beta)})$ is a symmetric tridiagonal (quasi-)cyclic matrix of the form

$$\tilde{\mathcal{C}}_{\alpha} = \begin{pmatrix} a_1 & b_1 & & b_L \\ b_1 & a_2 & \ddots & \\ & \ddots & \ddots & b_{L-1} \\ b_L & & b_{L-1} & a_L \end{pmatrix}, \quad (33)$$

with matrix elements

$$a_{\ell>1} = \mu_{\ell}^{-} + z_{\ell-1}^2 \mu_{\ell-1}^{+}, \quad (34a)$$

$$b_{\ell<L} = -\frac{z_{\ell}}{(t_{\ell})_{-}}, \quad (34b)$$

and the special cases concerning whether the couplings in the perpendicular direction are periodic, anti-periodic, or open,

$$a_1 = \mu_1^{-} + \alpha^2 z_L^2 \mu_L^{+}, \quad (35a)$$

$$b_L = -\alpha \frac{z_L}{(t_L)_{-}}. \quad (35b)$$

Here we have introduced the convenient abbreviation

$$y_{\pm} \equiv \frac{1}{2} (y^{-1} \pm y), \quad (36)$$

for an arbitrary quantity y , as well as

$$\mu_{\ell}^{\pm}(\varphi_m^{(\beta)}) = \frac{(t_{\ell})_{+}}{(t_{\ell})_{-}} \pm \cos \varphi_m^{(\beta)}, \quad (37)$$

which solely covers the $\varphi_m^{(\beta)}$ -dependency.

The matrix $\tilde{\mathcal{C}}_{\alpha}$ in (33) will be our starting point for the different BCs, but as we are hardly interested in the case of every line having a different coupling, we will apply the changes due to the according boundary conditions and then frankly assume homogenous but still anisotropic couplings. The determinant of a matrix of the form (33) can be easily calculated with a 2×2 transfer matrix *ansatz*, namely

$$\det \tilde{\mathcal{C}}_{\alpha} = \text{tr} [\mathcal{T}_L \cdots \mathcal{T}_2 \mathcal{T}_1] - 2(-1)^L \prod_{\ell=1}^L b_{\ell}, \quad (38)$$

while for $b_L = 0$ the formula simplifies to

$$\det \tilde{\mathcal{C}}_{\alpha} = \langle 0, 1 | \mathcal{T}_L \cdots \mathcal{T}_2 \mathcal{T}_1 | 1, 0 \rangle, \quad (39)$$

with the transfer matrices ($b_0 \equiv b_L$)

$$\mathcal{T}_{\ell} = \begin{pmatrix} a_{\ell} & -b_{\ell-1}^2 \\ 1 & 0 \end{pmatrix}. \quad (40)$$

Luckily the b_ℓ are all negative, giving an additional factor $(-1)^L$ to (38) and thus eliminating the dependency on whether L is even or odd. Thus our results are correct for arbitrary integer L and M .

If we assume translational invariance in both directions, we may reduce the coupling matrices further to $\mathbf{z}^\perp = z^\perp \mathbf{1}$ and $\mathbf{z}^\parallel = z^\parallel \mathbf{1}$ and diagonalise the perpendicular direction, too. Then the determinant becomes

$$\det \mathcal{A}_{\alpha\beta} = \prod_{m=0}^{M-1} \prod_{\ell=0}^{L-1} \det \begin{pmatrix} 0 & 1+z^\parallel e^{i\varphi_m^{(\beta)}} & -1 & -1 \\ -1-z^\parallel e^{-i\varphi_m^{(\beta)}} & 0 & 1 & -1 \\ 1 & -1 & 0 & 1+z^\perp e^{i\varphi_\ell^{(\alpha)}} \\ 1 & 1 & -1-z^\perp e^{-i\varphi_\ell^{(\alpha)}} & 0 \end{pmatrix} \quad (41a)$$

$$= \prod_{m=0}^{M-1} \prod_{\ell=0}^{L-1} 4z^\perp z^\parallel \left(z_+^\perp z_+^\parallel - z_-^\perp \cos \varphi_m^{(\alpha)} - z_-^\parallel \cos \varphi_\ell^{(\beta)} \right), \quad (41b)$$

which is just the result by McCoy & Wu for the anisotropic torus [11].

3 Scaling theory

The two-dimensional Ising model is one of the simplest systems showing a temperature-driven continuous phase transitions in the absence of a bulk magnetic field. Albeit this work focuses on the two-dimensional case, the following statements can be generalised for $d > 2$. We assume an $L \times M$ rectangular system, where L is its extend in the direction *perpendicular* (\perp) and M the extend in *parallel* (\parallel) direction for reasons that will be clear later on. In the vicinity of the phase transition the thermal fluctuations of the medium become long-ranged, but by imposing some sort of BCs, even (anti-)periodicity, they are confined by the geometry. The reduced free energy² for translationally invariant BCs $\beta \in \{\mathbf{p}, \mathbf{a}\}$ in parallel and α in perpendicular direction, $F^{(\alpha,\beta)} = -\ln Z^{(\alpha,\beta)}$ (again in units of $k_B T$), may be decomposed into an infinite volume term and a residual contribution [35, 36]

$$F^{(\alpha,\beta)}(L, M) = F_\infty^{(\alpha)}(L, M) + F_{\infty, \text{res}}^{(\alpha,\beta)}(L, M), \quad (42)$$

where the former term describes the behaviour in the thermodynamic limit $L, M \rightarrow \infty$, while the latter one covers the finite-size effects. Another way to decompose the free energy is into contributions $F_b^{(\beta)}$ for the bulk, $F_s^{(\alpha,\beta)}$ for the two surfaces, and $F_{\text{st}, \text{res}}^{(\alpha,\beta)}$ for the respective strip finite-size part as

$$F^{(\alpha,\beta)}(L, M) = \underbrace{L F_b^{(\beta)}(M) + F_s^{(\alpha,\beta)}(M)}_{F_{\text{st}}^{(\alpha,\beta)}(L, M)} + F_{\text{st}, \text{res}}^{(\alpha,\beta)}(L, M), \quad (43)$$

see Figure 4. Here, $F_{\text{st}}^{(\alpha,\beta)}(L, M)$ describes the strip limit $L \rightarrow \infty$ with M fixed, cf. [35, 36]. Combining those two decompositions splits the contributions further, namely the bulk free energy per slice $F_b^{(\beta)}$ reads

$$F_b^{(\beta)}(M) = M f_b + F_{b, \text{res}}^{(\beta)}(M), \quad (44)$$

²In the following we will omit the explicit dependency on the temperature T .

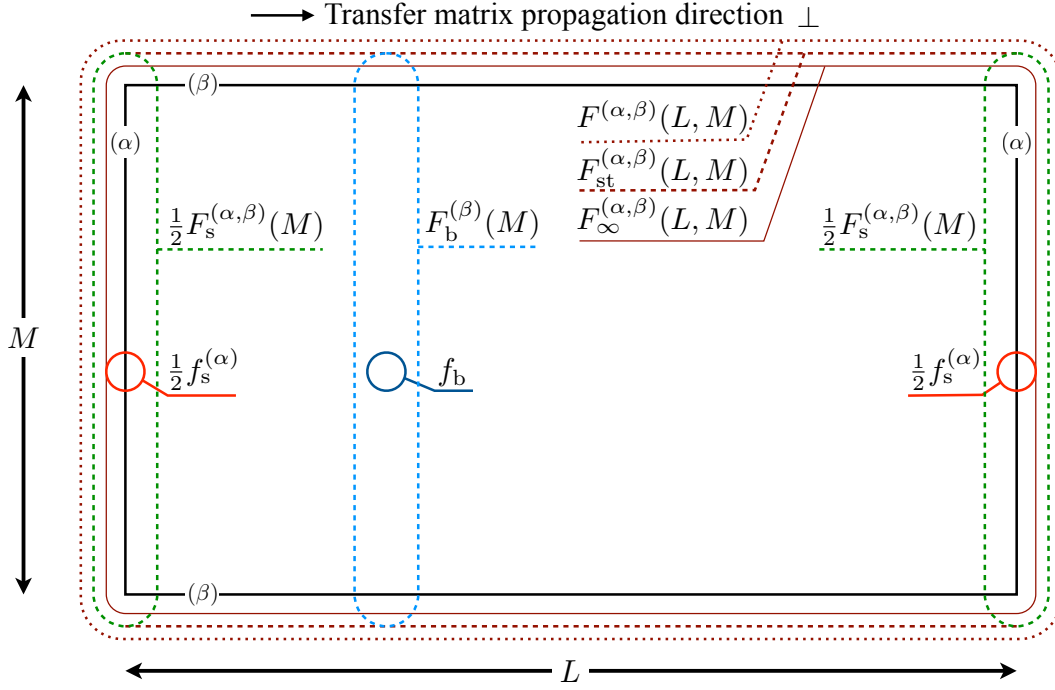


Figure 4: The BC β is either periodic or antiperiodic, BCs α can be periodic, antiperiodic, open, + or -. The free Energy $F(L, M)$ (dotted line) can be decomposed into various contributions as described in the text. The black rectangle represents the system with BCs α and β , while other solid lines mark infinite volume free energy densities independent of the systems lengths. On the contrary the dashed lines denote free energies containing some residual finite-size contribution.

with the bulk free energy density f_b and residual part $F_{b,\text{res}}^{(\beta)}$. Analogously, we find for the surface

$$F_s^{(\alpha,\beta)}(M) = M f_s^{(\alpha)} + F_{s,\text{res}}^{(\alpha,\beta)}(M), \quad (45)$$

with the surface free energy density $f_s^{(\alpha)}$ and the according residual free energy $F_{s,\text{res}}^{(\alpha,\beta)}(M)$. Both terms depend explicitly on the BC α (e.g., open boundaries or surface fields), while the residual contribution also accounts for the BC β , as these define the discrete spectrum for the finite system. Thus we can rewrite the two contributions in (42) as

$$F_{\infty}^{(\alpha)}(L, M) = LM f_b + M f_s^{(\alpha)}, \quad (46a)$$

$$F_{\infty,\text{res}}^{(\alpha,\beta)}(L, M) = L F_{b,\text{res}}^{(\beta)}(M) + F_{s,\text{res}}^{(\alpha,\beta)}(M) + F_{\text{st},\text{res}}^{(\alpha,\beta)}(L, M), \quad (46b)$$

cf. [36]. Note that it is possible to impose boundaries in more than one direction, introducing edges and corners and suitable contributions depending on the dimension of the hypercuboid; for the two dimensional case of the Ising model on the open rectangle the necessary calculations were done lately with the dimer approach presented above in [35, 36], and within the spinor representation in [8].

3.1 General scaling behaviour

Nevertheless, all residual contributions vanish in the thermodynamic limit for $T \neq T_c$, but near criticality the bulk correlation length in direction δ diverges as

$$\xi_\delta^{(\infty)}(\tau) \stackrel{\tau \geq 0}{\simeq} \hat{\xi}_\delta \tau^{-\nu}, \quad (47)$$

where $\tau = T/T_c - 1$ is the reduced temperature and $\hat{\xi}_\delta$ is the correlation length amplitude in the unordered phase, while ν is the according scaling exponent, with $\nu = 1$ for the two-dimensional case. In this small region around $T = T_c$ the residual free energy $F_{\infty, \text{res}}^{(\alpha, \beta)}$ only depends on the two length ratios $L/\xi_\perp^{(\infty)}(\tau)$ and $M/\xi_\parallel^{(\infty)}(\tau)$, where we assume the bulk correlation length amplitudes differ depending on the direction because of the anisotropic couplings. Following Fisher and de Gennes, the residual free energy thus fulfils the scaling *ansatz*

$$F_{\infty, \text{res}}^{(\alpha, \beta)}(L, M) \simeq \Theta^{(\alpha, \beta)}(x_\perp, x_\parallel), \quad (48)$$

where $\Theta^{(\alpha, \beta)}$ is the total residual free energy scaling function, depending on the two temperature scaling variables

$$x_\perp \equiv \tau \left(\frac{L}{\hat{\xi}_\perp} \right)^{1/\nu} \quad \text{and} \quad x_\parallel \equiv \tau \left(\frac{M}{\hat{\xi}_\parallel} \right)^{1/\nu}, \quad (49)$$

which are connected by the reduced aspect ratio

$$\rho \equiv \frac{L/\hat{\xi}_\perp}{M/\hat{\xi}_\parallel} \quad (50)$$

via the relation

$$x_\perp = \rho^{1/\nu} x_\parallel. \quad (51)$$

Sometimes it is advantageous to use a volume scaling function depending on a volume-like scaling variable

$$x_\circ \equiv \tau \left(\frac{LM}{\hat{\xi}_\perp \hat{\xi}_\parallel} \right)^{1/(2\nu)}. \quad (52)$$

Consequently, we may change our focus onto either one of the two directions or the volume and rewrite the scaling functions accordingly into a perpendicular (\perp), a parallel (\parallel), or a volume (\circ) form

$$F_{\infty, \text{res}}^{(\alpha, \beta)}(L, M) \simeq \Theta_\circ^{(\alpha, \beta)}(x_\circ, \rho) = \rho^{-1} \Theta_\perp^{(\alpha, \beta)}(x_\perp, \rho) = \rho \Theta_\parallel^{(\alpha, \beta)}(x_\parallel, \rho). \quad (53)$$

The critical Casimir force is defined as derivative of the residual free energy with respect to the according system length, e. g. in perpendicular direction,

$$\mathcal{F}_C^{(\alpha, \beta)}(L, M) \equiv -\frac{1}{M} \frac{\partial}{\partial L} F_{\infty, \text{res}}^{(\alpha, \beta)}(L, M) \quad (54)$$

and analogously to (53) scales as

$$\mathcal{F}_C^{(\alpha, \beta)}(L, M) \simeq (LM)^{-1} \vartheta_\circ^{(\alpha, \beta)}(x_\circ, \rho) = L^{-2} \vartheta_\perp^{(\alpha, \beta)}(x_\perp, \rho) = M^{-2} \vartheta_\parallel^{(\alpha, \beta)}(x_\parallel, \rho). \quad (55)$$

The residual free energy and the Casimir force scaling functions are connected by the relations

$$\vartheta_{\perp}^{(\alpha,\beta)}(x_{\perp}, \rho) = - \left[-1 + \frac{x_{\perp}}{\nu} \frac{\partial}{\partial x_{\perp}} + \rho \frac{\partial}{\partial \rho} \right] \Theta_{\perp}^{(\alpha,\beta)}(x_{\perp}, \rho), \quad (56a)$$

$$\vartheta_{\parallel}^{(\alpha,\beta)}(x_{\parallel}, \rho) = - \left[1 + \rho \frac{\partial}{\partial \rho} \right] \Theta_{\parallel}^{(\alpha,\beta)}(x_{\parallel}, \rho), \quad (56b)$$

$$\vartheta_{\circ}^{(\alpha,\beta)}(x_{\circ}, \rho) = - \left[\frac{x_{\circ}}{2\nu} \frac{\partial}{\partial x_{\circ}} + \rho \frac{\partial}{\partial \rho} \right] \Theta_{\circ}^{(\alpha,\beta)}(x_{\circ}, \rho). \quad (56c)$$

In the following we will focus on the scaling function $\Theta_{\parallel}^{(\alpha,\beta)}(x_{\parallel}, \rho)$ for the parallel direction as it arises naturally within our calculations from the product in (22). Just like the residual free energy can be decomposed into its bulk, surface, and strip contribution in (46b), the scaling function consist of such parts, which can be written as

$$\rho \Theta_{\parallel}^{(\alpha,\beta)}(x_{\parallel}, \rho) = \rho \Theta_{\text{b}}^{(\beta)}(x_{\parallel}) + \Theta_{\text{s}}^{(\alpha,\beta)}(x_{\parallel}) + \Psi^{(\alpha,\beta)}(x_{\parallel}, \rho) \quad (57)$$

with

$$LF_{\text{b,res}}^{(\beta)}(M) \simeq \rho \Theta_{\text{b}}^{(\beta)}(x_{\parallel}), \quad (58a)$$

$$F_{\text{s,res}}^{(\alpha,\beta)}(M) \simeq \Theta_{\text{s}}^{(\alpha,\beta)}(x_{\parallel}), \quad (58b)$$

$$F_{\text{st,res}}^{(\alpha,\beta)}(L, M) \simeq \Psi^{(\alpha,\beta)}(x_{\parallel}, \rho). \quad (58c)$$

For the torus and the other systems with translational invariance in both directions there is no surface and thus $\Theta_{\text{s}}^{(\alpha,\beta)}(x_{\parallel}) \equiv 0$ for $\alpha, \beta \in \{\text{p}, \text{a}\}$, all other cases will be discussed in the second part of the paper.

3.2 Anisotropic scaling

Now we need to discuss the influence of the *weakly anisotropic* couplings on the scaling behaviour. Here the critical point expands to a critical line as we may rewrite the condition of criticality [37] as

$$\sinh(2K^{\perp}) \sinh(2K^{\parallel}) = 1 \quad \Leftrightarrow \quad t = z, \quad (59)$$

which again becomes a point by fixing the couplings by a factor κ as

$$K^{\parallel} = \kappa K^{\perp}. \quad (60)$$

In terms of t and z this becomes

$$t = (z^*)^{\kappa}, \quad (61)$$

and we can identify the critical point with the equation

$$z_{\text{c}}(\kappa) = \left[\frac{1 - z_{\text{c}}(\kappa)}{1 + z_{\text{c}}(\kappa)} \right]^{\kappa}. \quad (62)$$

The correlation lengths along the two directions read [11]

$$\xi_{\perp}^{(\infty)}(z, t) = \left(\ln \coth K^{\perp} - 2K^{\parallel} \right)^{-1} = \ln^{-1} \frac{t}{z}, \quad (63a)$$

$$\xi_{\parallel}^{(\infty)}(z, t) = \left(\ln \coth K^{\parallel} - 2K^{\perp} \right)^{-1} = \ln^{-1} \frac{z^*}{t^*}, \quad (63b)$$

with the dual couplings $t^* = (1 - t)/(1 + t)$ and $z^* = (1 - z)/(1 + z)$, see (24). This form emphasises the choice of the reduced temperatures in the two directions as

$$\tau_{\perp} = \frac{t}{z} - 1 \quad \text{and} \quad \tau_{\parallel} = \frac{z^*}{t^*} - 1. \quad (64)$$

The amplitude ratio $r_{\xi} = \hat{\xi}_{\perp}/\hat{\xi}_{\parallel}$ can also be rewritten as

$$r_{\xi}^{-1} \simeq [z_c(\kappa)]_-, \quad (65)$$

and thus the scaling variables read

$$x_{\perp} \equiv L\tau, \quad (66a)$$

$$x_{\parallel} \equiv r_{\xi}^{-1} M\tau, \quad (66b)$$

which gives the correct relation $x_{\perp} = \rho x_{\parallel}$, see [38].

A problem arises when due to high anisotropy the relevant length scale changes, e.g., $L/M < 1$ but $\rho > 1$ or vice versa. Then the scaling behaviour of the system changes dramatically. For even larger anisotropy the systems starts to decouple its lines (or rows, depending on the direction which is coupled the strongest) and finally decomposes into one dimensional independent subsystems.

4 The torus

Albeit the toroidal geometry differs from all other BCs discussed later on as its the only one without a surface, we will first turn toward it here. After we have calculated the partition function on the finite lattice, we will carve out the bulk properties and calculate its thermodynamic limit. Afterwards we will see how the dimer approach and the choice of signs distinguishes between periodicity and anti-periodic BCs as a consequence of its interplay with the directed graph being subject to the Pfaffian.

Let us return to (33), for which we now assume independent homogeneity in both directions, i.e., $z_{\ell} \equiv z \forall \ell$ and $t_{\ell} \equiv t \forall \ell$, as well as $\mu_{\ell}^{\pm}(\varphi) \equiv \mu^{\pm}(\varphi) \forall \ell$. Then it is comfortable to factorise the homogeneous factor z/t_{-} leaving every non-zero off-diagonal element but b_L equal to -1 . Due to this procedure, additionally the diagonal entries simplify to

$$\frac{t_{-}}{z} (\mu^{-} + z^2 \mu^{+}) = 2(t_{+} z_{+} - t_{-} z_{-} \cos \varphi), \quad (67)$$

which can be parameterised into the anisotropic Onsager dispersion

$$\cosh \gamma_m^{(\beta)} \equiv t_{+} z_{+} - t_{-} z_{-} \cos \varphi_m^{(\beta)}. \quad (68)$$

Thus the matrix for the torus has the form

$$\mathcal{C}_L^{(\alpha)}(\varphi_m^{(\beta)}) = \begin{pmatrix} 2 \cosh \gamma_m^{(\beta)} & -1 & & -\alpha \\ -1 & 2 \cosh \gamma_m^{(\beta)} & \ddots & \\ & \ddots & \ddots & -1 \\ -\alpha & & -1 & 2 \cosh \gamma_m^{(\beta)} \end{pmatrix}, \quad (69)$$

which is connected to (33) by

$$\det \tilde{\mathcal{C}}_\alpha(\varphi_m^{(\beta)}) = \left(\frac{z}{t_-} \right)^L \det \mathcal{C}_L^{(\alpha)}(\varphi_m^{(\beta)}). \quad (70)$$

To calculate the determinant, we use the transfer matrix approach (38)

$$\det \mathcal{C}_L^{(\alpha)}(\varphi_m^{(\beta)}) = \text{tr} [\mathcal{T}^L(\gamma_m^{(\beta)})] - 2\alpha(-1)^{2L} \quad (71)$$

with the transfer matrix

$$\mathcal{T}(\gamma_m^{(\beta)}) = \begin{pmatrix} 2 \cosh \gamma_m^{(\beta)} & -1 \\ 1 & 0 \end{pmatrix}. \quad (72)$$

The eigenvalues of \mathcal{T} are $e^{\pm \gamma_m^{(\beta)}}$ and, depending on $\alpha = \pm 1$, the determinant thus reads

$$\det \mathcal{C}_L^{(\alpha)}(\varphi_m^{(\beta)}) = \left(e^{\frac{L}{2} \gamma_m^{(\beta)}} - \alpha e^{-\frac{L}{2} \gamma_m^{(\beta)}} \right)^2. \quad (73)$$

In the following we will omit the superscript of the γ , since the parity is encoded in the product over either even or odd numbers. Having said that, we denote the parity in the other direction with \pm to account for the dependency on α , and thus we use

$$Z_{e/o}^\pm = \prod_{\substack{0 \leq m < 2M \\ m \text{ even/odd}}} \left(e^{\frac{L}{2} \gamma_m} \pm e^{-\frac{L}{2} \gamma_m} \right), \quad (74)$$

where we have incorporated the square root of (5). Then the non-regular part of the partition function reads

$$\frac{Z^{(\mathbf{p}, \mathbf{p})}}{Z_0^{(\mathbf{p}, \mathbf{p})}} = \frac{1}{2} \left(\frac{2t^* z}{t_-} \right)^{ML/2} [Z_o^+ + Z_o^- + Z_e^+ - \text{sgn}(t - z) Z_e^-], \quad (75)$$

where the $\text{sgn}(t - z)$ stems from the root in (5), too, and assures that for arbitrary anisotropy κ the contribution is a monotonic function in temperature. This can be easily understood by looking at the critical value of Z_e^- : There $\gamma_0 = 0$ and thus one of the factors becomes zero, but as we have taken the square root in (75), we have to correct the according sign.

4.1 Bulk and finite-size contribution

In section 3 we discussed how the free energy of a finite system may be decomposed into summands describing the different contributions from volume, surfaces, and finiteness. As a

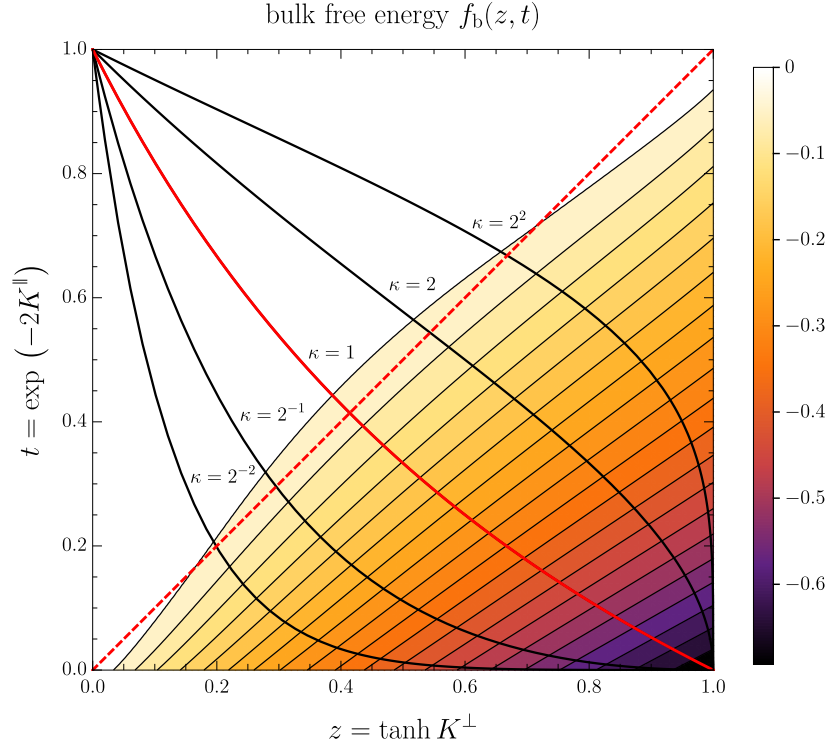


Figure 5: Bulk free energy density $f_b(z, t)$. The dashed line marks criticality for arbitrary anisotropy $\kappa = K^\perp/K^\parallel$. For fixed anisotropy the two couplings are connected by $t = (z^*)^\kappa$, see (61), and the black lines mark the run of the according curve, where the isotropic case $\kappa = 1$ is shown in red.

matter of fact, the toroidal geometry has no surfaces and thus the aforementioned decomposition includes only the bulk contribution and the finite-size part. Therefore it is perfectly suitable to identify the former one and calculate its thermodynamic limit.

We start by splitting the $Z_{e/o}^\pm(L, M)$ into their exponentially growing and decaying parts as

$$Z_{e/o}^\pm = p_{e/o}^\pm(L, M) \prod_{\substack{0 \leq m < 2M \\ m \text{ even/odd}}} e^{\frac{L}{2} \gamma_m}, \quad (76)$$

with

$$p_{e/o}^\pm(L, M) = \prod_{\substack{0 \leq m < 2M \\ m \text{ even/odd}}} (1 \pm e^{-L \gamma_m}). \quad (77)$$

Now we may factorise the odd product over the leading exponential in (75) from *all four* contributions, as it is slightly larger than the one over the even numbers. The according bulk part of the free energy then simply reads

$$F_b^{(p)}(M) = -\frac{M}{2} \left(\ln \frac{2t^* z}{t_-} - \frac{1}{M} \sum_{\substack{0 \leq m < 2M \\ m \text{ odd}}} \gamma_m \right), \quad (78)$$

thus leaving the residual part as

$$F_{\text{st, res}}^{(\mathbf{p}, \mathbf{p})}(L, M) = -\ln \left[(p_o^+ + p_o^-) + (p_e^+ \mp p_e^-) \prod_{m=0}^{2M-1} e^{(-1)^m \frac{L}{2} \gamma_m} \right]. \quad (79)$$

To calculate the bulk contribution to the free energy in the thermodynamic limit

$$f_b(t, z) \equiv \lim_{M \rightarrow \infty} M^{-1} F_b^{(\mathbf{p})}(M) \quad (80)$$

we use the Euler-Maclaurin sum formula to obtain the integral representation

$$f_b(z, t) = -\frac{1}{2} \ln \frac{2t^* z}{t_-} - \frac{1}{4\pi} \int_0^{2\pi} d\varphi \gamma(\varphi) \quad (81)$$

and omit all corrections of $\mathcal{O}(M^{-1})$ or higher. Fig. 5 shows the bulk free energy density as function of the two coupling variables z and t . For the isotropic critical case we find

$$f_b(z_c, z_c) = -\ln(1 - z_c) - \frac{2G}{\pi}, \quad (82)$$

where G is Catalan's constant.

4.2 Scaling form

As discussed in Sec. 3, in a finite system there is always not only a residual contribution present, but this contribution can be split up into different parts as well. We start with the scaling form of γ as it is the central quantity for the toroidal geometry, afterwards we will first calculate the residual bulk free energy scaling function and then the one for the residual strip free energy. Therefore we introduce the hyperbolic parametrisation based on the scaling form of γ , which allows us to regularise the arising terms properly. At criticality the bulk residual scaling function coincides with the change of the free energy of the according conformal field theory due to the projection from the plane onto the cylinder.

For the scaling limit of γ we start with the definition for the anisotropic temperature scaling variables in (64) and (66) and solve them for z and t to get the somehow unhandy formulas

$$t(r_\xi, M; x_\parallel) = \frac{1}{r_\xi} \left(1 + \frac{x_\parallel}{2M} \right) \left[\sqrt{1 + r_\xi^2 \frac{1 + \frac{x_\parallel}{r_\xi M}}{(1 + \frac{x_\parallel}{2M})^2}} - 1 \right], \quad (83a)$$

$$z(r_\xi, M; x_\parallel) = \frac{t(r_\xi, M; x_\parallel)}{1 + \frac{x_\parallel}{r_\xi M}}. \quad (83b)$$

Now we use them in (68) together with $\varphi = \Phi/M$, substitute $M = \epsilon^{-1}$ and expand $\cos(\epsilon \Phi)$ up to the second order in ϵ around $\epsilon = 0$ to obtain

$$\cosh \gamma = 1 + \frac{\epsilon^2}{2} \frac{\Gamma^2 + \epsilon x_\parallel \Phi^2}{r_\xi^2 + \epsilon r_\xi x_\parallel} + \mathcal{O}(\epsilon^4), \quad (84)$$

where we have introduced

$$\Gamma = \sqrt{x_{\parallel}^2 + \Phi^2}. \quad (85)$$

With a Puiseux series expansion around $\epsilon = 0$,

$$\operatorname{arcosh} \left(1 + \frac{y^2}{2} \right) = y + \mathcal{O}(y^3), \quad (86)$$

we finally find, with $L = \rho r_{\xi} M$,

$$L\gamma(\varphi) \simeq \rho \lim_{\epsilon \rightarrow 0} \left(\frac{\Gamma^2 + \epsilon x_{\parallel} \Phi^2}{1 + \epsilon \frac{x_{\parallel}}{r_{\xi}}} \right)^{1/2} = \rho \Gamma. \quad (87)$$

As we made only the most general assumptions, we can use this result through out the whole rest of this work.

Now we will turn to the characteristic polynomials (21). Their scaling form is quite simple as we only have to replace $\varphi = \Phi/M$ to obtain

$$\mathcal{P}_e^{\pm}(\Phi) = e^{\pm i\Phi} - 1, \quad (88a)$$

$$\mathcal{P}_o^{\pm}(\Phi) = e^{\pm i\Phi} + 1, \quad (88b)$$

where the \pm accounts for the two possible choices of the eigenvalue $e^{\pm i\varphi_m^{(\beta)}}$ in (19). This freedom is essential to the regularisation of the residual free energies, because if we assume Φ to be complex to calculate the sum in terms of contour integrals, $\mathcal{P}_{e/o}^+(\Phi)$ diverges in the lower and $\mathcal{P}_{e/o}^-(\Phi)$ diverges in the upper half-plane. To avoid these divergences we simply switch between the two possible realisations if we somewhere cross the real axis. We obtain suitable counting polynomials for the even and odd sums as integration kernel from the logarithmic derivative of the $\mathcal{P}_{e/o}^{\pm}(\Phi)$ as

$$\mathcal{K}_e^{\pm}(\Phi) = \partial_{\Phi} \ln \mathcal{P}_e^{\pm}(\Phi) = +\frac{1}{2} \left[\cot \frac{\Phi}{2} \pm i \right], \quad (89a)$$

$$\mathcal{K}_o^{\pm}(\Phi) = \partial_{\Phi} \ln \mathcal{P}_o^{\pm}(\Phi) = -\frac{1}{2} \left[\tan \frac{\Phi}{2} \mp i \right], \quad (89b)$$

and consequently for the alternating sum

$$\delta\mathcal{K}(\Phi) = \partial_{\Phi} \ln \frac{\mathcal{P}_e^{\pm}(\Phi)}{\mathcal{P}_o^{\pm}(\Phi)} = \csc \Phi, \quad (89c)$$

without any distinction for the upper and lower half-plane, as the divergences cancel each other.

Looking closely at (85) we see that we can parametrise this hyperbolic equation by

$$\Phi = |x_{\parallel}| \sinh \omega, \quad (90a)$$

$$\Gamma = |x_{\parallel}| \cosh \omega, \quad (90b)$$

solving the equation for all $\omega \in \mathbb{C}$. Note that this is the critical limiting case of the elliptic parametrisation of (68), which is used off criticality for finite systems for more complex BCs, e.g., for the open rectangle.

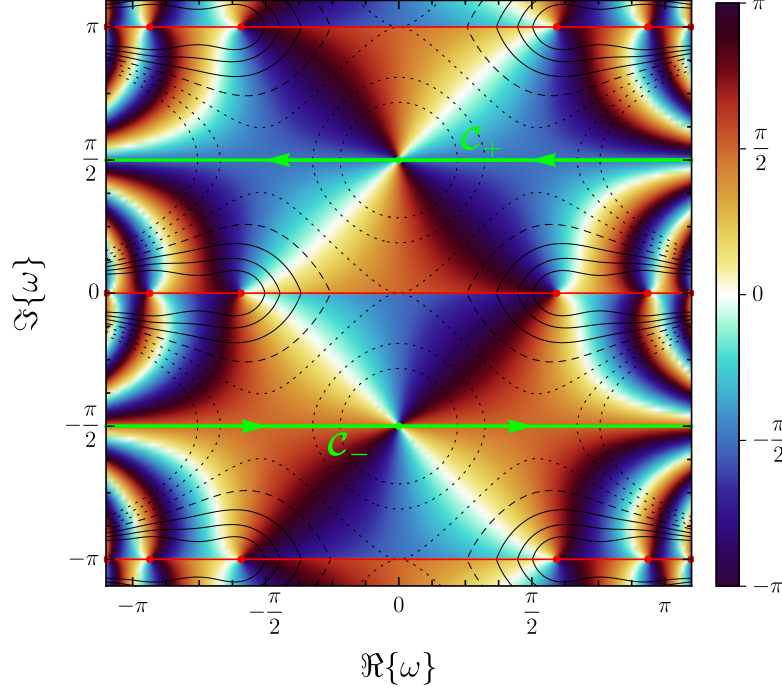


Figure 6: Complex structure of the integrand of (92). The two contours \mathcal{C}_+ in the upper and \mathcal{C}_- in the lower half-plane are connected by non-contributing paths at $\Re\{\omega\} \rightarrow \pm\infty$ to form the closed contour \mathcal{C} . The complex phase is colour coded from $-\pi$ to π , while the lines of constant absolute value c are shown as black dotted ($c < 1$), dashed ($c = 1$) or solid ($c > 1$) lines ranging from 2^{-3} to 2^{+3} . The zeros at $\omega = \pm i\pi/2$ are marked as green dots, while the poles on the lines with $\Im\{\omega\} = n\pi$, $n \in \mathbb{Z}$, are marked as red dots. Additionally, the phase jump due to the different choices for the counting polynomial for the upper and lower half-plane are marked as red lines. Note that due to the transformation into the hyperbolic ω -plane the structure is 2π -periodic along the imaginary axis. The contributions along the paths \mathcal{C}_+ and \mathcal{C}_- are the same, as the phase in the upper half-period is reversed with respect to the lower half-period.

Combining (87), (89b) and (90) we now have the tools to calculate the scaling function of the residual bulk free energy

$$F_{\text{res,b}}^{(\text{p})}(M) = F_{\text{b}}^{(\text{p})}(M) - Mf_{\text{b}} = \frac{M}{4\pi} \int_0^{2\pi} d\varphi \gamma(\varphi) - \frac{1}{2} \sum_{\substack{0 \leq m < 2M \\ m \text{ odd}}} \gamma_m. \quad (91)$$

By rewriting the sum as contour integral over Γ with the counting polynomial \mathcal{K}_0^\pm and substituting the hyperbolic parametrisation we get

$$\Theta_{\text{b}}^{(\text{p})}(x_{\parallel}) = -\frac{1}{4i\pi} \oint_{\mathcal{C}} d\omega x_{\parallel}^2 \cosh^2 \omega \mathcal{K}_0^\pm(|x_{\parallel}| \sinh \omega). \quad (92)$$

Note that the additional term $\pm i$ in \mathcal{K}_0^\pm can be interpreted as the integral in (91) for the bulk

free energy, as

$$\lim_{\Phi \rightarrow \pm i\infty} \tan \frac{\Phi}{2} = \pm i \quad (93)$$

and thus a shift of the integration path along the imaginary axis can be interpreted as smooth interpolation between the sum on the real axis and the integral at infinity, which is mapped onto the lines at $\pm i\pi/2$ within the hyperbolic parametrisation. The integrand is shown in Fig. 6 together with an appropriately chosen contour. For $|\Phi| \rightarrow \infty$ the integrand vanishes, thus making the integral over the paths $\Im\{\omega\} = \pm\pi/2$ the only relevant parts of the contour, which are equal as they only differ by a phase of π . This leaves us with

$$\Theta_b^{(p)}(x_{\parallel}) = \frac{1}{2i\pi} \int_{-\infty}^{\infty} d\omega x_{\parallel}^2 \sinh^2 \omega \frac{i}{2} \left[\tanh \left(\frac{|x_{\parallel}|}{2} \cosh \omega \right) - 1 \right] \quad (94a)$$

$$= \frac{1}{4\pi} \int_{-\infty}^{\infty} d\Phi \frac{\Phi^2}{\Gamma} \left[\tanh \frac{\Gamma}{2} - 1 \right] \quad (94b)$$

$$= -\frac{1}{2\pi} \int_{-\infty}^{\infty} d\Phi \ln [1 + e^{-\Gamma}], \quad (94c)$$

where we first resubstituted to the Φ -plane and then integrated by parts, reproducing the result from [32] calculated for the isotropic case.

A similar procedure will be our way to go in every upcoming calculation, that is, use the according counting polynomial as integral kernel in the contour integral representation of the sum, transform it into the hyperbolic parametrisation, shift the integration path to $\Im\{\omega\} = \pm\pi/2$, and perform the integration. Applying this scheme to the alternating sum in the exponent of (79),

$$\frac{L}{2} \sum_{m=0}^{2M-1} (-1)^m \gamma_m \simeq \rho \delta\Theta_b(x_{\parallel}), \quad (95)$$

then gives us

$$\delta\Theta_b(x_{\parallel}) = \frac{1}{4i\pi} \int_C d\omega x_{\parallel}^2 \cosh^2 \omega \delta\mathcal{K}(|x_{\parallel}| \sinh \omega) \quad (96a)$$

$$= \frac{1}{2\pi} \int_{-\infty}^{\infty} d\Phi \frac{\Phi^2}{\Gamma} \operatorname{csch} \Gamma \quad (96b)$$

$$= -\frac{1}{2\pi} \int_{-\infty}^{\infty} d\Phi \ln \left[\frac{1 - e^{-\Gamma}}{1 + e^{-\Gamma}} \right], \quad (96c)$$

again reproducing the result of [32]. Note that the alternating sum regularises itself and thus there is only the well known kernel for alternating sums present, which is shown in Fig. 7 in the same manner as Fig. 6.

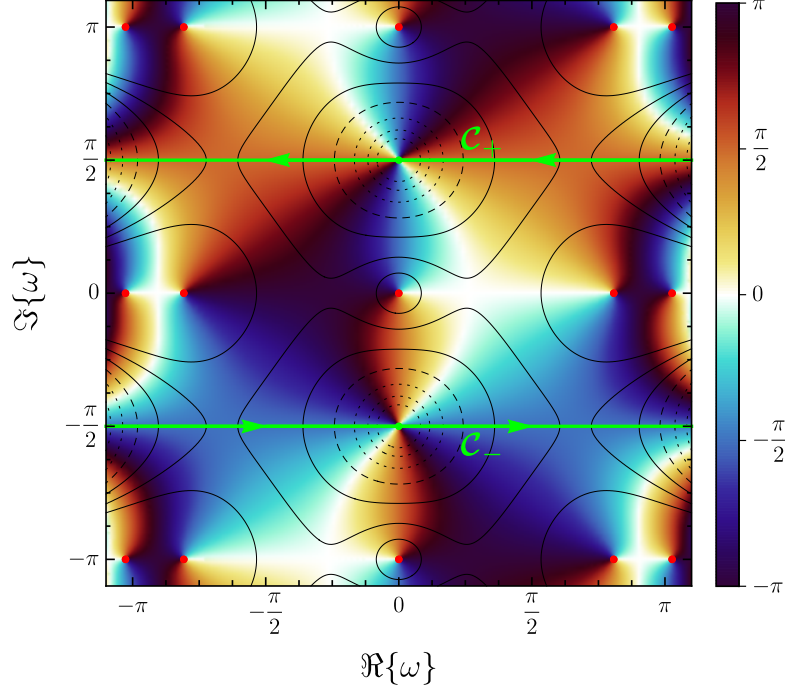


Figure 7: Complex structure of the alternating sum over the Γ_m in the hyperbolic ω -plane (integrand of (96a)), together with the contour $\mathcal{C} = \mathcal{C}_+ + \mathcal{C}_-$. Here no phase jump is present and the 2π -periodicity along the imaginary axis is continuous, but nevertheless the upper and lower contour are equal due to the reversed phase in the upper and lower half-period.

Finally we have to calculate the scaling limit of the $p_{e/o}^\pm(L, M)$, which is really straight forward, as we only have to expand the product symmetrically to infinity and replace $L\gamma$ by its scaling form. Thus we get

$$p_{e/o}^\pm(L, M) \simeq P_{e/o}^\pm(x_\parallel, \rho) \quad (97)$$

with

$$P_{e/o}^\pm(x_\parallel, \rho) = \prod_{\substack{m=-\infty \\ m \text{ even/odd}}}^{\infty} (1 \pm e^{-\rho \Gamma_m}), \quad (98)$$

where we have used the discrete form of Γ with

$$\Gamma_m = \sqrt{x_\parallel^2 + \Phi_m^2} \quad (99)$$

with $\Phi_m = m\pi$, and used the symmetries of γ_m with respect to $m = 0$ and $m = M$ to expand the product symmetric around zero. Now we combine them into an even and an odd scaling function

$$\Psi_e^{(p,p)}(x_\parallel, \rho) = \ln 2 - \ln [P_e^+(x_\parallel, \rho) - \text{sgn}(x_\parallel) P_e^-(x_\parallel, \rho)], \quad (100a)$$

$$\Psi_o^{(p,p)}(x_\parallel, \rho) = \ln 2 - \ln [P_o^+(x_\parallel, \rho) + P_o^-(x_\parallel, \rho)], \quad (100b)$$

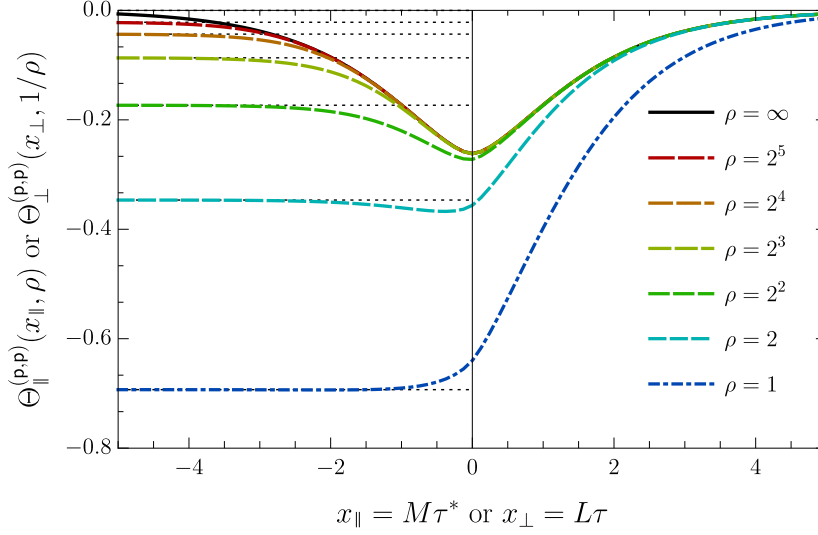


Figure 8: Scaling function $\Theta_\mu^{(p,p)}(x_\mu, \rho)$ for different values for the aspect ratio ρ . Due to the periodic BCs the system has the symmetry $\Theta_\parallel^{(p,p)}(x_\parallel, \rho) = \Theta_\perp^{(p,p)}(x_\perp, 1/\rho)$. The limit (104) for $x_\mu \rightarrow -\infty$ due to the degeneracy is shown for according values of ρ as dotted lines.

and calculate the analogue of an alternating strip contribution

$$\delta\Psi^{(p,p)}(x_\parallel, \rho) = \Psi_e^{(p,p)}(x_\parallel, \rho) - \Psi_o^{(p,p)}(x_\parallel, \rho). \quad (101)$$

Eventually we find the scaling function for the torus to be

$$\Theta_\parallel^{(p,p)}(x_\parallel, \rho) = \Theta_b^{(p)}(x_\parallel) + \rho^{-1} \Psi_o^{(p,p)}(x_\parallel, \rho) - \rho^{-1} \ln \left[1 + e^{-\rho \delta\Theta_b(x_\parallel) - \delta\Psi^{(p,p)}(x_\parallel, \rho)} \right], \quad (102)$$

which has some remarkable properties. First and for most this form shows the symmetry $\Theta_\parallel^{(p,p)}(x_\parallel, \rho) = \Theta_\perp^{(p,p)}(x_\perp, 1/\rho)$, as $\Theta_b^{(p)}$ and $\Psi_o^{(p,p)}$ as well as $\delta\Theta_b$ and $\delta\Psi^{(p,p)}$ exchange their roles under this transformations, which may be seen best in the two limiting cases

$$\Theta_\parallel^{(p,p)}(x_\parallel, \rho \rightarrow \infty) = \Theta_b^{(p)}(x_\parallel), \quad (103a)$$

$$\Theta_\perp^{(p,p)}(x_\perp, \rho \rightarrow 0) = \Theta_b^{(p)}(x_\perp), \quad (103b)$$

where for the latter one P_o^+ becomes dominant near $x_\perp = 0$ and equal to P_o^- for $|x_\perp| \gg 1$, thus $\Psi_o^{(p,p)}$ can be written as integral in terms of the Euler-Maclaurin formula. Additionally the last term of (102) is only important for finite ρ and even dominant in the vicinity of $\rho = 1$ with

$$\lim_{x_\parallel \rightarrow -\infty} \ln \left[1 + e^{-\rho \delta\Theta_b(x_\parallel) - \delta\Psi^{(p,p)}(x_\parallel, \rho)} \right] = \ln 2, \quad (104)$$

which stems from the different order of the limits in the scaling regime and the thermodynamic limit. While in an infinitely large system as supposed by the latter one, the system is frozen in either of the two possible magnetised states because a transition would require infinitely much energy, the finiteness of the system in the scaling limit allows such a transition, resulting in a factor 2 in the partition function and thus this topological contribution in the scaling function. However, whenever this symmetry is broken, e. g., by a surface field, this contribution is not present and the scaling functions decay to zero for $|x_\mu| \rightarrow \infty$.

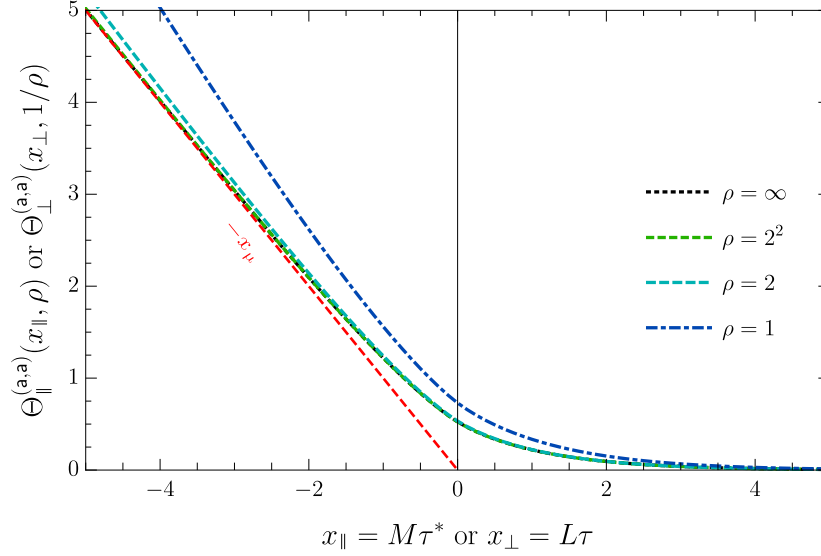


Figure 9: Scaling function $\Theta_{\mu}^{(a,a)}(x_{\mu}, \rho)$ for different values for the aspect ratio ρ . Due to the antiperiodic BCs the system has the symmetry $\Theta_{\parallel}^{(a,a)}(x_{\parallel}, \rho) = \Theta_{\perp}^{(a,a)}(x_{\perp}, 1/\rho)$. For negative values of x_{μ} the scaling function diverges linearly, marked as red (dark) dashed line. The scaling function converges very fast to its limiting form at $\rho = \infty$, while its biggest contribution is at $\rho = 1$ as there the domain wall lies diagonal in the system and is thus longest compared to the two length scales L and M .

4.3 (Anti-)Periodicity and surface tension

Let us now turn back to the finite systems solution using the dimer approach and consider antiperiodic boundary conditions in the parallel direction, i.e., $\sigma_{\ell,m} \equiv -\sigma_{\ell,m+M}$. They can be implemented as one line of anti-ferromagnetic parallel couplings, which corresponds to a change in the orientation of the oriented lattice concerning this particular line within the dimer representation. Here we need to emphasise that the oriented graph from the dimer mapping is absolutely independent of the choice of sign of any coupling. Nevertheless, changing the sign of *all* couplings in one row (or column) can be interpreted as reversing the direction of all corresponding edges and leaving the couplings unchanged. We now may choose the line, which imposes these BCs to be the line concerning the handling of the transition circles in the Pfaffian. Since we already need all four combinations of orientations, this procedure thus only exchanges the role of $Z_{e/o}^{+}$ and $Z_{e/o}^{-}$. Consequently, if we impose antiperiodic BCs in the perpendicular direction, i.e., $\sigma_{\ell,m} \equiv -\sigma_{\ell+L,m}$, the roles of Z_e^{\pm} and Z_o^{\pm} are exchanged. Tab. 1 shows which of the $Z_{e/o}^{\pm}$ contributes with a minus sign depending on the BCs.

Of course this directly transfers to the scaling functions, which are shown in Figs. 9, 10, and 11. Just like the case of periodic BCs in both directions, antiperiodic BCs (denoted (a, a) in the superscript) in both directions impose a symmetry according to

$$\Theta_{\parallel}^{(a,a)}(x_{\parallel}, \rho) = \Theta_{\perp}^{(a,a)}(x_{\perp}, 1/\rho), \quad (105)$$

see, Fig. 9, where the two combinations of periodic and anti-periodic BCs (denoted (p, a) and

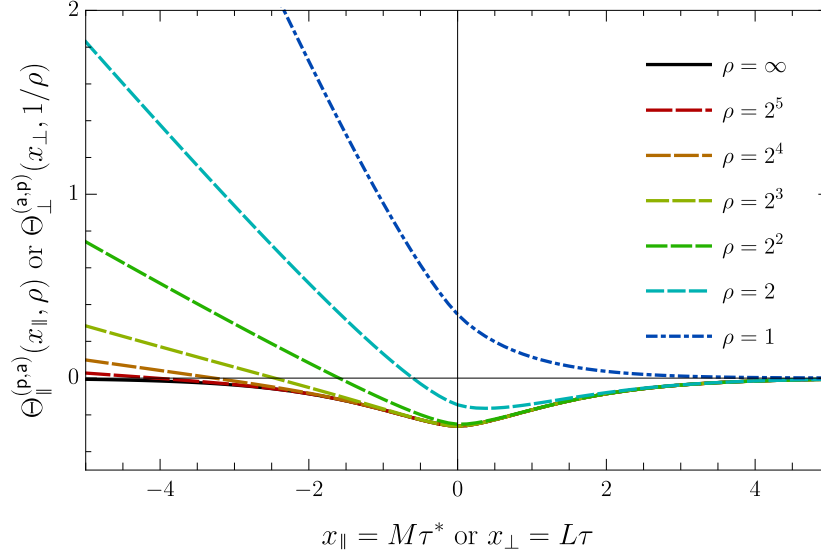


Figure 10: Scaling functions $\Theta_{||}^{(p,a)}(x_{||}, \rho)$ and due to the symmetry $\Theta_{\perp}^{(a,p)}(x_{\perp}, 1/\rho)$ for different values for the aspect ratio ρ . Here the domain wall forms along the short direction of the system and thus the limiting case is $\Theta_b^{(p)}(x_{\mu})$.

(a, p) are connected via

$$\Theta_{||}^{(a,p)}(x_{||}, \rho) = \Theta_{\perp}^{(p,a)}(x_{\perp}, 1/\rho), \quad (106a)$$

$$\Theta_{||}^{(p,a)}(x_{||}, \rho) = \Theta_{\perp}^{(a,p)}(x_{\perp}, 1/\rho), \quad (106b)$$

see Figs. 10 and 11.

An important consequence of an antiperiodic boundary is the formation of a domain wall and thus a surface tension contribution σ to the free energy. This contribution can be calculated as difference between the free energy of the system with antiperiodic and the one of the system with periodic boundaries in the same direction

$$\sigma^{(a,p)}(L, M) = F^{(a,p)}(L, M) - F^{(p,p)}(L, M), \quad (107)$$

or alternatively as quotient of the according partition functions. Thus any bulk or surface contribution cancels out and what is left is the free energy of the domain wall composed of

Table 1: Sign of the contributions $Z_{e/o}^{\pm}$ according to which combination of periodic (p) and antiperiodic (a) boundary conditions in parallel and perpendicular direction are imposed.

BCs	Z_e^-	Z_e^+	Z_o^-	Z_o^+
(p, p)	−	+	+	+
(p, a)	+	−	+	+
(a, p)	+	+	−	+
(a, a)	+	+	+	−

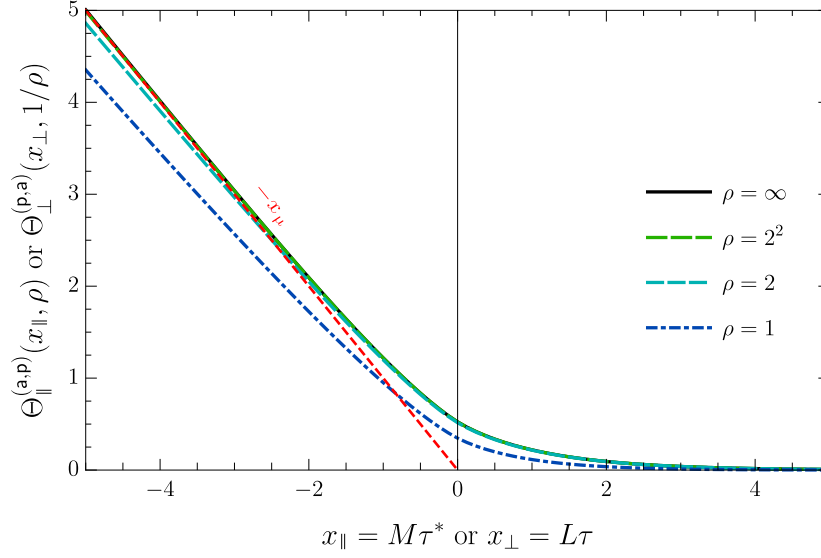


Figure 11: Scaling functions $\Theta_{\parallel}^{(a,p)}(x_{\parallel}, \rho)$ and due to the symmetry $\Theta_{\perp}^{(p,a)}(x_{\perp}, 1/\rho)$ for different values for the aspect ratio ρ . Here the domain wall forms along the long direction of the system and thus the limiting case is $\Sigma_b^{(a)}(x_{\mu})$ with a linear divergence for $x_{\mu} \rightarrow -\infty$, see (110).

the differences of the according residual finite-size parts, which consequently fulfils the scaling *ansatz*

$$\sigma^{(a,p)}(L, M) \simeq \rho \Sigma_{\parallel}^{(a,p)}(x_{\parallel}, \rho) \quad (108)$$

with the scaling function

$$\Sigma_{\parallel}^{(a,p)}(x_{\parallel}, \rho) = \Theta_{\parallel}^{(a,p)}(x_{\parallel}, \rho) - \Theta_{\parallel}^{(p,p)}(x_{\parallel}, \rho). \quad (109)$$

Likewise, the surface tension and its scaling function are obtained for periodic/antiperiodic and antiperiodic/antiperiodic BCs. For all three cases the scaling functions diverge linearly in the according scaling variable x_{μ} , where μ might either be the parallel or the perpendicular direction, in the ordered phase for a growing length of the domain wall, as depicted in Figs. 9, 10, and 11. The limiting case for a dominating domain wall, i. e., antiperiodic boundaries in the long direction, reads

$$\Sigma_b^{(a)}(x_{\mu}) = \delta \Theta_b(x_{\mu}) - x_{\mu} H(-x_{\mu}), \quad (110)$$

where $\Sigma_b^{(a)}(x_{\mu})$ is the bulk contribution to the surface tension, cf. [12], and $H(x)$ is the Heaviside step function with $H(x) \equiv \partial_x \max\{0, x\}$.

5 Conclusion

We presented a systematic calculation of the free energy scaling functions for various anisotropic systems with translationally invariant boundary conditions. Therefor we started with the commonly known dimer representation of the two-dimensional Ising model, which we recapitulated

in some detail to show the connection between the Pfaffian representation and the boundary conditions of the underlying system. Using the coupling constant z and its dual counterpart t turned out to be beneficial for the calculation, as it compresses the formulas to a clearly arranged form. The calculation of the necessary Pfaffians of the original $4LM \times 4LM$ matrices was condensed down to a straight forward formalism for periodic and antiperiodic boundaries assuming translational invariance in one direction. Within this approach we implemented an anisotropic scaling theory and showed analytically that a weak anisotropy can be absorbed into a generalised aspect ratio ρ . For the transition from the finite system to the scaling form we introduced the hyperbolic parametrisation of the scaling form of the Onsager dispersion, which is the scaling limit of the elliptic parametrisation of finite systems. The results are in perfect agreement with former calculations, but the method is far more general and we will use it to apply boundary fields to the open cylinder in the subsequent part of this paper.

Acknowledgements

We like to thank Malte Henkel for helpful discussions and inspirations.

Funding information This work was partially supported by the Deutsche Forschungsgemeinschaft through Grant HU 2303/1-1.

References

- [1] L. Onsager, *Crystal statistics. I. A two-dimensional model with an order-disorder transition*, Phys. Rev. **65**, 117 (1944), doi:10.1103/PhysRev.65.117.
- [2] B. Widom, *Equation of state in the neighborhood of the critical point*, The Journal of Chemical Physics **43**(11), 3898 (1965), doi:10.1063/1.1696618.
- [3] L. P. Kadanoff, *Scaling laws for Ising models near T_c* , Physics **2**(6), 263 (1966).
- [4] A. M. Polyakov, *Conformal symmetry of critical fluctuations*, JETP Lett. **12**, 381 (1970).
- [5] J. L. Cardy, *Conformal invariance and universality in finite-size scaling*, J. Phys. A: Math. Gen. **17**(7), L385 (1984), doi:10.1088/0305-4470/17/7/003.
- [6] J. Cardy, *Boundary conformal field theory*, In J.-P. Francoise, G. L. Naber and T. S. Tsun, eds., *Encyclopedia of Mathematical Physics*, pp. 333 – 340. Academic Press, Oxford, ISBN 978-0-12-512666-3, doi:10.1016/B0-12-512666-2/00398-9 (2006).
- [7] G. Bimonte, T. Emig and M. Kardar, *Conformal field theory of critical Casimir interactions in 2D*, EPL **104**(2), 21001 (2013), doi:10.1209/0295-5075/104/21001.
- [8] R. J. Baxter, *The bulk, surface and corner free energies of the square lattice Ising model*, Journal of Physics A: Mathematical and Theoretical **50**(1), 014001 (2017), doi:10.1088/1751-8113/50/1/014001.
- [9] B. Kaufman, *Crystal statistics. II. Partition function evaluated by spinor analysis*, Phys. Rev. **76**, 1232 (1949), doi:10.1103/PhysRev.76.1232.

- [10] M. E. Fisher, *On the dimer solution of planar Ising models*, Journal of Mathematical Physics **7**(10), 1776 (1966), doi:10.1063/1.1704825.
- [11] B. M. McCoy and T. T. Wu, *The Two-Dimensional Ising Model*, Dover Books on Physics. Dover Publication, Inc., Mineola, New York, 2 edn., ISBN 978-0-486-49335-0 (2014).
- [12] H. Hobrecht and A. Hucht, *Anisotropic scaling of the two-dimensional Ising model II: Surfaces and boundary fields*, To be published (2018).
- [13] H. B. G. Casimir and D. Polder, *The influence of retardation on the London-van der Waals forces*, Phys. Rev. **73**, 360 (1948), doi:10.1103/PhysRev.73.360.
- [14] H. B. G. Casimir, *On the attraction between two perfectly conducting plates*, Proc. K. Ned. Akad. Wet. **51**, 793 (1948).
- [15] M. E. Fisher and P.-G. de Gennes, *Phénomènes aux parois dans un mélange binaire critique*, C. R. Acad. Sci. Paris, Ser. B **287**, 207 (1978).
- [16] R. Garcia and M. H. W. Chan, *Critical fluctuation-induced thinning of ^4He films near the superfluid transition*, Phys. Rev. Lett. **83**, 1187 (1999), doi:10.1103/PhysRevLett.83.1187.
- [17] A. Hucht, *Thermodynamic Casimir effect in ^4He films near T_λ : Monte Carlo results*, Phys. Rev. Lett. **99**, 185301 (2007), doi:10.1103/PhysRevLett.99.185301.
- [18] R. Garcia and M. H. W. Chan, *Critical Casimir effect near the ^3He - ^4He tricritical point*, Phys. Rev. Lett. **88**, 086101 (2002), doi:10.1103/PhysRevLett.88.086101.
- [19] M. Fukuto, Y. F. Yano and P. S. Pershan, *Critical Casimir effect in three-dimensional Ising systems: Measurements on binary wetting films*, Phys. Rev. Lett. **94**, 135702 (2005), doi:10.1103/PhysRevLett.94.135702.
- [20] C. Hertlein, L. Helden, A. Gambassi, S. Dietrich and C. Bechinger, *Direct measurement of critical Casimir forces*, Nature **451**, 172 (2008), doi:10.1038/nature06443.
- [21] M. Krech, *Casimir forces in binary liquid mixtures*, Phys. Rev. E **56**, 1642 (1997), doi:10.1103/PhysRevE.56.1642.
- [22] H. W. Diehl, D. Grüneberg, M. Hasenbusch, A. Hucht, S. B. Rutkevich and F. M. Schmidt, *Exact thermodynamic Casimir forces for an interacting three-dimensional model system in film geometry with free surfaces*, EPL **100**(1), 10004 (2012), doi:10.1209/0295-5075/100/10004.
- [23] H. W. Diehl, D. Grüneberg, M. Hasenbusch, A. Hucht, S. B. Rutkevich and F. M. Schmidt, *Large- n approach to thermodynamic Casimir effects in slabs with free surfaces*, Phys. Rev. E **89**, 062123 (2014), doi:10.1103/PhysRevE.89.062123.
- [24] E. Eisenriegler and U. Ritschel, *Casimir forces between spherical particles in a critical fluid and conformal invariance*, Phys. Rev. B **51**, 13717 (1995), doi:10.1103/PhysRevB.51.13717.
- [25] T. W. Burkhardt and E. Eisenriegler, *Casimir interaction of spheres in a fluid at the critical point*, Phys. Rev. Lett. **74**, 3189 (1995), doi:10.1103/PhysRevLett.74.3189.

- [26] P. D. Francesco, P. Mathieu and D. Sénéchal, *Conformal Field Theory*, Springer-Verlag New York, Inc., ISBN 0-387-94785-X (1997).
- [27] D. Simmons-Duffin, *A semidefinite program solver for the conformal bootstrap*, Journal of High Energy Physics **2015**(6), 174 (2015), doi:10.1007/JHEP06(2015)174.
- [28] O. Vasilyev, A. Gambassi, A. Maciolek and S. Dietrich, *Universal scaling functions of critical Casimir forces obtained by Monte Carlo simulations*, Phys. Rev. E **79**, 041142 (2009), doi:10.1103/PhysRevE.79.041142.
- [29] H. Hobrecht and A. Hucht, *Direct simulation of critical Casimir forces*, EPL **106**(5), 56005 (2014), doi:10.1209/0295-5075/106/56005, arXiv:1405:4088.
- [30] H. Hobrecht and A. Hucht, *Many-body critical Casimir interactions in colloidal suspensions*, Phys. Rev. E **92**, 042315 (2015), doi:10.1103/PhysRevE.92.042315.
- [31] J. R. Edison, N. Tasios, S. Belli, R. Evans, R. van Roij and M. Dijkstra, *Critical Casimir forces and colloidal phase transitions in a near-critical solvent: A simple model reveals a rich phase diagram*, Phys. Rev. Lett. **114**, 038301 (2015), doi:10.1103/PhysRevLett.114.038301.
- [32] H. Hobrecht and A. Hucht, *Critical Casimir force scaling functions of the two-dimensional Ising model at finite aspect ratios*, Journal of Statistical Mechanics: Theory and Experiment **2017**(2), 024002 (2017), doi:10.1088/1742-5468/aa5280.
- [33] A. E. Ferdinand and M. E. Fisher, *Bounded and inhomogeneous Ising models. I. Specific-heat anomaly of a finite lattice*, Phys. Rev. **185**, 832 (1969), doi:10.1103/PhysRev.185.832, There is a typo in Eq. (3.36), the term $\xi S_1(n)\tau^2/2$ is missing.
- [34] A. Hucht, D. Grüneberg and F. M. Schmidt, *Aspect-ratio dependence of thermodynamic Casimir forces*, Phys. Rev. E **83**, 051101 (2011), doi:10.1103/PhysRevE.83.051101.
- [35] A. Hucht, *The square lattice Ising model on the rectangle I: finite systems*, J. Phys. A: Math. Theor. **50**(6), 065201 (2017), doi:10.1088/1751-8121/aa5535.
- [36] A. Hucht, *The square lattice Ising model on the rectangle II: finite-size scaling limit*, J. Phys. A: Math. Theor. **50**(26), 265205 (2017), doi:10.1088/1751-8121/aa6b7a.
- [37] H. A. Kramers and G. H. Wannier, *Statistics of the two-dimensional ferromagnet. Part I*, Phys. Rev. **60**(252–262) (1941), doi:10.1103/PhysRev.60.252.
- [38] A. Hucht, *On the symmetry of universal finite-size scaling functions in anisotropic systems*, J. Phys. A: Math. Gen. **35**(31), L481 (2002), doi:10.1088/0305-4470/35/31/103.